

Experimental Parameter Determination and Laboratory Verification of the Inverse Hysteresis Model for Single-Phase Toroidal Transformers

Carlos H. Alonso¹, Saeed Jazebi^{1,2}, and Francisco de León¹, *Fellow, IEEE*

¹Department of Electrical, and Computer Engineering, New York University, Brooklyn, NY 11201 USA

²Applied Materials Inc., Gloucester, MA 01930 USA

This paper presents a laboratory test procedure to determine the parameters of the inverse hysteresis model (IHM) applicable to single-phase toroidal transformer low-frequency modeling. The model parameters are obtained through a fitting procedure of the history-independent IHM of a series of open-circuit experiments and waveform recordings. These experiments can be easily executed during the transformer acceptance testing at the factory laboratory. The performance of the model is verified under various operational conditions, such as sinusoidal excitation, varied frequencies and voltages, and non-sinusoidal excitations. The results show that the model performs very well under all tested conditions giving great confidence that the proposed method can be used for parameter determination.

Index Terms—Excess losses, inverse hysteresis model (IHM), quasi-static hysteresis measurement, transformer modeling.

I. INTRODUCTION

MAGNETIC hysteresis is a complex phenomenon that occurs in the iron core of electrical machines. Hysteresis models can be classified into two categories: 1) static (rate independent) [1]–[7] and 2) dynamic (rate dependent) [1]–[3], [8], [9]. Static models describe the behavior of the ferromagnetic materials as a function of excitation magnitude and in some models their magnetization history. In contrast, dynamic models take into account the rate of change of excitation, its waveform, and its effects on loss mechanisms such as wall displacements and domain rotation. These effects are represented as eddy currents and excess losses. The foundation of several dynamic models is a reliable static model. A dynamic model can be created by adding components to an existing static model. Therefore, an accurate and easy way to implement a static model is significant for the proper representation of losses in a dynamic hysteresis model.

Hysteresis is modeled in different ways and such models can be used with others, which represent specific operational conditions such as inrush and saturation [1]. For example, Gruosso and Repetto [4] and Dick and Watson [5] have modeled hysteresis using simple circuit elements such as switches, capacitors, and backlash inductors. Some models predict the operation point based on the distance of the reversal point to a major loop and assume a function that predicts how that distance evolves [2], [3], [6], [7]. There are also models that need to be tuned (fitted) for every operation state such as different frequencies [9]. Some of them are neither easy to implement nor have a broad set of applications [1], [9]. This can be especially seen in direct models compared with

inverse models. Direct models describe $B(H)$ relations, while inverse models use $H(B)$ making them better suited for the voltage driven operation of power systems. However, there are more accurate models, and despite their limitations, some of these models are widely used because of their simplicity and flexibility for different applications [1], [5], [6], [10].

The dynamic model with three components proposed in [3], [7], and [8] is relatively simple to code and implement. A comprehensive description on how to use this model in the Electromagnetic Transients Program is given in these papers. This dynamic model can be used for a wide range of applications such as the study of low-frequency electromagnetic transients, non-sinusoidal excitation, and calculation of losses with a voltage excitation at different levels and frequencies [6]. The model is described by three components: 1) a quasi-static inverse hysteresis model (IHM); 2) an eddy current model; and 3) an excess losses model as follows:

$$H(B, \dot{B}) = H_{\text{stat}}(B) + H_{\text{cl}}(B, \dot{B}) + H_{\text{exc}}(B, \dot{B}) \quad (1)$$

where H , H_{stat} , H_{cl} , and H_{exc} are the instantaneous dynamic, static, classical eddy, and excess magnetic field components, respectively, for a given flux density B and flux rate of change \dot{B} . Even when the flux density B is a function of time $B(t)$, H_{stat} is not considered a function of time because it depends only on the instantaneous value of B and its history, but not on its rate of change, as do the other components of (1).

The starting point of most of the aforementioned models is the availability of a quasi-static hysteresis loop of the ferromagnetic material used to build the transformer model. In this paper, such a quasi-static loop is reconstructed from measurements taken at the transformer terminals. Currently, several techniques to measure the quasi-static loops exist [11], [12]. Unfortunately, equipment to trace it, especially for soft materials, is neither common nor simple to operate [5]. In addition, sophisticated techniques are used by transformer manufacturers to minimize air gaps aiming to reduce the no-load losses

Manuscript received April 27, 2016; revised June 9, 2016 and July 2, 2016; accepted July 2, 2016. Date of publication July 13, 2016; date of current version October 17, 2016. Corresponding author: C. H. Alonso (e-mail: cha258@nyu.edu).

Color versions of one or more of the figures in this paper are available online at <http://ieeexplore.ieee.org>.

Digital Object Identifier 10.1109/TMAG.2016.2591000

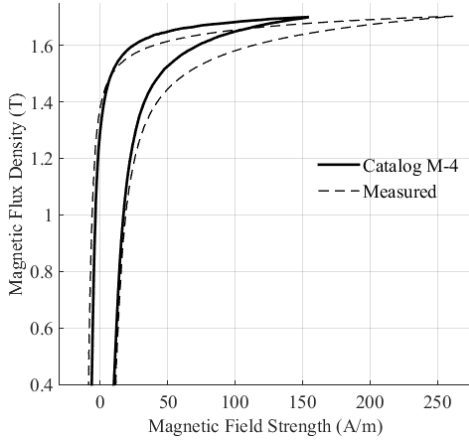


Fig. 1. B - H characteristic measured from the terminal of a toroidal transformer built with an M-4 material at 1 Hz versus the catalog quasi-static loop. One can see that the manufacturing processes have damaged the magnetic properties.

and magnetizing current; yet, air gaps are unavoidable. Hence, even if the quasi-static hysteresis loop of the ferromagnetic material is available, the actual loop (seen from terminals) for a particular transformer is different. Fig. 1 compares the B - H curve, as measured from terminals on a flux driven regime (at 1.7 T) of a toroidal transformer at 1 Hz built with an M-4 material, with the catalog [13] quasi-static loop.

The objective of this paper is to present a simple procedure to compute the parameters required to build the IHM for single-phase transformer cores using terminal measurements. The method is simpler than the traditional tracers of [11] and [12]. Deeper attention is paid in this paper to the IHM component since it is the foundation of the dynamic hysteresis model. The parameter determination process proposed in this paper uses common (or doable) terminal tests at 50 or 60 Hz at different voltages. To obtain a good model, the measurement of only three loops is strictly necessary. Naturally, with a larger number of measurements, a better model can be produced. Furthermore, the procedure presented does not rely on the transformer design data.

In Section V, a step-by-step example is presented for illustration. Finally, in Section VI, the model is validated against measurements for different excitation levels and different frequencies using a toroidal transformer. We believe, however, that the method is applicable to most single-phase distribution transformers that have a behavior similar to the toroidal.

II. INVERSE HYSTERESIS MODEL

The process presented in this paper is suitable for grain-oriented (GO) materials such as the common M-4. B - H curves are used in this paper instead of λ - i curves to show material properties rather than the characteristics of a particular transformer. This allows drawing more general conclusions for the behavior of the iron core independent of the construction of the transformer. The toroidal transformer used in this paper is rated at 1 kVA, 120:120 V, and is built with an M-4 core. The core dimensions are inner diameter = 8.57 cm, outer diameter = 14.92 cm, and height = 5.08 cm;

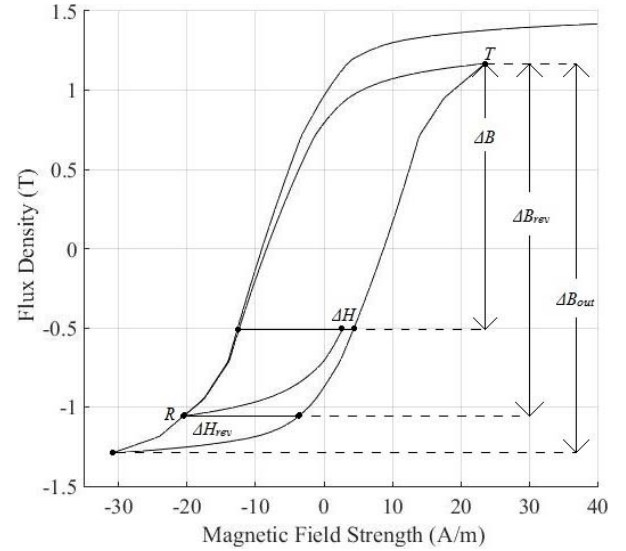


Fig. 2. Definitions of the parameters used in (2)-(7).

giving a cross-sectional area of 16.13 cm². Each winding has 196 turns of 13 AWG wire.

The IHM (both history dependent and independent) is characterized by the largest quasi-static cycle, known as the major loop (that can be obtained from catalogs [13], measurement, or reconstruction), along with the following set of equations that predict how the magnetic field strength behaves [3]:

$$H_{\text{stat}}(B) = H_{a+d}(B) - \Delta H(x) \quad (2)$$

where H_{a+d} is the ascending or descending magnetic field strength on the major loop at a given B and ΔH is the distance between the outer loop (which may be the major loop; see below) and the predicted magnetic field strength at a given B , which the model computes as

$$\Delta H(x) = \Delta H_R \cdot (1 - b)x e^{-a(1-x)} + \delta \cdot \Delta H_{\text{out}}(B) \cdot bx^{y_6} \quad (3)$$

where ΔH_{out} is the width of the outer loop at flux B . ΔH_R is the distance of the magnetic field strength from the reversal point to the corresponding outer ascending or descending branch expressed as

$$\Delta H_R = H_{a+b}(B_R) - H(B_R). \quad (4)$$

Coefficients a and b are given by

$$a = |\Delta B_{\text{rev}}| \cdot (y_0 + y_1\beta + y_2\beta^2 + y_3\beta^3) \quad (5)$$

$$b = y_4(1 - \beta)^{y_5} \quad (6)$$

where y_0, y_1, \dots, y_6 are fitting coefficients obtained through a minimization procedure as explained in Section III-B, ΔB_{rev} is the flux density difference between the reversal flux (point R in Fig. 2) and the tip flux (point T in Fig. 2) of the loop where the flux is moving toward, B_R is the reversal flux, and x, β , and δ are defined as follows:

$$x = \frac{\Delta B}{\Delta B_{\text{rev}}}, \quad \beta = \frac{\Delta B_{\text{rev}}}{\Delta B_{\text{out}}}, \quad \delta = \frac{\Delta H_R}{\Delta H_{\text{rev}}} \quad (7)$$

where ΔB is the flux distance between the instantaneous flux and the flux tip of the loop where the flux is moving toward, ΔB_{out} is the distance of the tip and lowest fluxes of the ascending and descending branches, respectively (the height of the outer loop). ΔH_{rev} is the magnetic field strength distance between the ascending and descending branches at the reversal flux (ΔH_{rev} and ΔH_R are the same for the history-independent model). The incremental variables ΔH , ΔH_{rev} , ΔB , ΔB_{rev} , and ΔB_{out} are graphically defined in Fig. 2.

The model is history independent if these distances are in relation with the major loop and it is history dependent if they are functions of the last ascending and descending branches.

To avoid negative slopes and trajectories that go beyond the major loop, the constraints $a > 0$, $0 \leq b \leq 1$, and $y_6 > 0$ have to be imposed for all $0 \leq \beta \leq 1$, as indicated in [3] and [7].

Although the history-dependent model is more realistic, there are several reasons to use a history-independent model for the calculation of parameters.

- 1) The coefficients in (2)–(7) are the same for both models.
- 2) The history-independent model is easier to program.
- 3) The curves obtained to calculate the parameters start from the major loop. This means that they are first-order reversal curves (FORCs), which the history-independent IHM model is capable of predicting very accurately [3].

The IHM consists of two current components: the fast component, which is the exponential part of (3), and the slow component, which is proportional to b in (3). It is important to mention that (5) is slightly different from [3, eq. (10)]. This distance affects the slow component of the model except when $y_5 = 1$. In addition, (5) and (6) have a lower number of coefficients and a different structure compared with the approach of [7] assuring a positive b for all β . These changes make the model capable of adapting to different materials by assigning different weights to each component. Results are not presented because of lack of space.

III. PARAMETER DETERMINATION OF THE IHM

Coefficients y_0 – y_6 can be fitted if one is in possession of a major loop, with its ascending branch defined by at least four points, and a set of FORCs [7]. There is no minimum number of FORCs needed, but the larger the number is, the more accurate the model would be. Nevertheless, the procedure presented in this paper assumes that such information is not available; it will be obtained from measurements.

The method presented here derives a major loop, with its ascending branch characterized by a minimum of six points, and at least two FORCs. This is achieved with at least three dynamic hysteresis recordings at 60 Hz. If more resolution on the major loop and more FORCs is desired, the number of recorded dynamic loops needs to increase. The example shown in this paper uses ten recordings from 0.71 to 1.73 T.

A. Quasi-Static Major Loop

As was mentioned in Section I, there are several methods to get the quasi-static loop from direct measurements. It is more challenging to measure a quasi-static loop (at near zero frequency) than a loop at nominal frequency from

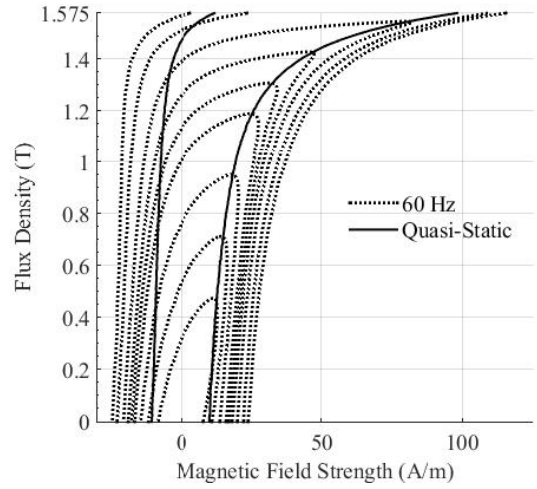


Fig. 3. Measured dynamic loops (dotted lines) for excitation levels from 0.47 to 1.73 T, together with the measured quasi-static loop (solid line) for a toroidal transformer built with an M-4 material.

terminal measurements. In this paper, to obtain the latter, the primary side of the transformer is energized and the secondary is left in open circuit. Digital recordings are taken from the primary current and secondary voltage (to exclude the voltage drop in the winding resistance) in steady state and referred to one side. Next, the secondary voltage is integrated to obtain the linkage flux. This is convenient because the frequency of the test is the same as the power system frequency. References [14] and [15] present procedures to trace 60 Hz hysteresis loops for iron samples difficult to implement in built transformers.

Fig. 3 shows the set of measured loops at 60 Hz (dotted lines) for excitation levels from 0.47 to 1.73 T for a toroidal transformer built with an M-4 material, which will be used to compute the quasi-static loop. In addition, Fig. 3 shows the measured quasi-static loop for 1.7 T at 1 Hz for the same transformer (to be used as reference to compare with the calculations). Note that the upper half of the quasi-static loop coincides with the tips of the measured B – H curves for flux densities above (but not including) 0.71 T.

We remark that at the peak the current is purely inductive ($\dot{B} = 0$). Therefore, neither eddy nor excess losses are present, isolating the hysteretic component of (1). It is recommended to use more measured loops near the ascending and descending knee points. Nevertheless, even when the quasi-static loop does not cross the dynamic peaks exactly at 0.71 and 0.47 T (in Fig. 3), the crossing is very close and such peaks may be useful. The decision on whether or not a point can be used is made by examining the reconstructed lower half part of the ascending branch (the derivation is presented at the end of this section). If the included point produces a section with a negative slope, such a point has to be neglected. Because of this, we observed that only the peaks starting at 0.71 T and above to the highest possible flux (especially under saturation) can be used to reconstruct the quasi-static loop. This is the reason why the peak point of the 0.47 T loop is not used in the computation.

In this test, voltage and flux are sinusoidal functions. Since flux is computed from the integration of the voltage, through

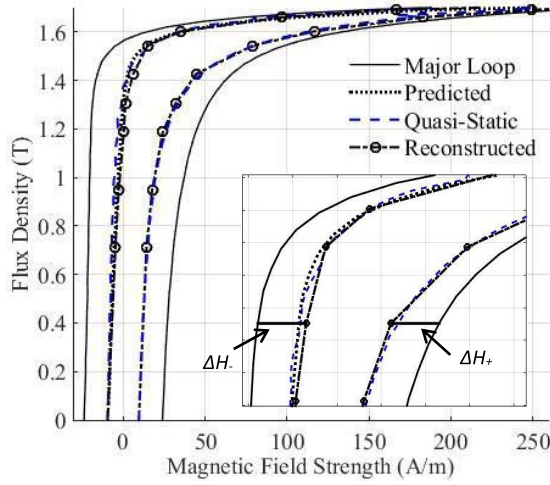


Fig. 4. Predicted descending upper half (dotted line), reconstructed quasi-static loop (dashed line with circles), and measured quasi-static loop (solid line). The predicted line is derived from the upper ascending branch of the measured quasi-static loop and the dynamic loop. The reconstructed loop is obtained only from 60 Hz measurements. Inset: a closer view of the knee region and graphical representations for ΔH_+ and ΔH_- , where both have the same magnitude at a given B .

Faraday's law, we have

$$V[\omega(t_0 + t)] = -V[\omega(t_0 - t)] \quad (8)$$

$$\lambda[\omega(t_{pk} + t)] = \lambda[\omega(t_{pk} - t)] \quad (9)$$

where t_0 is the instant when voltage crosses zero and t_{pk} is the point where the flux is at its peak value. We note that this situation happens when $t_0 = t_{pk}$.

To obtain the lower part of the ascending branch, it is necessary to first acquire the upper part of the descending branch, which is antisymmetric. The distance between H and H_{stat} could be computed from the three components of the dynamic model (1). The classical and excess fields in (1) are given by [2], [8]

$$H_{cl}(\dot{B}) = \frac{d^2}{12\rho} \frac{dB}{dt} \quad (10)$$

$$H_{exc}(B, \dot{B}) = \pm g(B) \left| \frac{dB}{dt} \right|^\alpha \quad (11)$$

where d is the lamination thickness, ρ is the material resistivity, $g(B)$ is a polynomial with even symmetry that represents the excess losses, α is a power coefficient for the excess losses (0.5 for most cases), and the \pm sign of the excess field is the sign of dB/dt . The procedure to obtain these parameters will be introduced in Section IV.

When at a given instant the operation point is on the upper half of the ascending branch, dB/dt and B are positive because $H > H_{stat}$ and the flux is building up. Then, subtracting the static component from (1), we have

$$H(B, \dot{B}) - H_a(B) = H_{cl}(\dot{B}) + H_{exc}(B, \dot{B}) = \Delta H_+. \quad (12)$$

This distance is called ΔH_+ and it is positive (see Fig. 4). Since $g(B)$ is an even function and the behavior indicated in (8) is the same for dB/dt and because the flux obeys (9), the

following expression is obtained for the descending branches:

$$H(B, -\dot{B}) - H_d(B) = -H_{cl}(\dot{B}) - H_{exc}(B, \dot{B}) = \Delta H_-. \quad (13)$$

Comparing (12) and (13) at the same level of flux density (B) in the descending branch (see the inset of Fig. 4), one can see that (12) and (13) have the same magnitude for the behavior implied in (8) and (9), respectively. The magnitude of the distance between the upper half of the dynamic loop ascending branch and the quasi-static loop is the same as the upper half of the dynamic loop descending branch to the quasi-static loop. This means that the upper half of the descending branch can be derived from (12) and (13) as follows:

$$H_d(B) = H_{dyn}(B, -\dot{B}) + \Delta H_+. \quad (14)$$

Because the ascending and descending branches of the quasi-static major loop are symmetrical about the origin, a transformation

$$-H_d(B) \rightarrow H_a(-B) \quad (15)$$

is done to obtain the lower half of the ascending branch. Therefore, this branch can also be obtained with the following calculation:

$$H_a(-B) = H(-B, \dot{B}) - \Delta H_+(B). \quad (16)$$

The major loop can be just characterized by a linear interpolation of the points that conform the ascending branch. To obtain the descending branch, (15) is applied in reverse direction to the former. Because of this, if N dynamic measurements are performed to obtain a quasi-static loop, such a loop will be characterized by $2N$ points. Fig. 4 validates this method by comparing the reconstruction made using two different measurements. One curve is the predicted descending branch (upper half) from a measured ascending (upper half) quasi-static branch. The other curve is obtained from a reconstruction of the whole quasi-static loop just from 60 Hz measurements at different magnitudes. The comparison (Fig. 4) shows a very good agreement.

It is noteworthy that the major loop is almost the same comparing the measured data and catalog information below 0.8 T (see Fig. 1). Therefore, if it is not feasible to obtain measurements at low excitations, the catalog data can be used to characterize the part of the loop close to the coercive field. Nevertheless, the dimensions of the core and the number of turns of the windings are required to transform the information to a λ - i loop. Finally, it is important to observe that the first and last points of the ascending branch, which define the reconstructed quasi-static hysteresis loop, are antisymmetric.

B. Calculation of Coefficients

Other necessary parameters are coefficients y_0 – y_6 . To obtain these parameters, a set of FORCs is needed. A set of minor quasi-static loops can be derived from the same measurements that were taken to reconstruct the major loop (see Fig. 5). This is achieved with the same process used to obtain the major loop, but instead of using all the measurements, one FORC is derived from all the measured loops that are lower

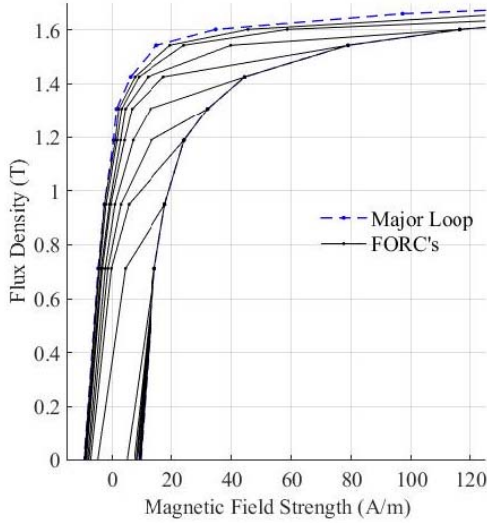


Fig. 5. Set of reconstructed FORCs for the M-4 transformer.

than the largest used for the last reconstructed quasi-static loop. For example, if ten measurements were carried out to derive the major loop, the nine lowest measurements are used to reconstruct the first FORC from top to bottom, then the eight lowest for the second FORC, and so on. Hence, from a total number of N measurements, the same number of quasi-static loops can be reconstructed (including the major loop). In addition, because minor loops start from the major loop, they are part of a set of FORCs, similar to the information presented in catalogs [13]. Consequently, they can be used in the fitting process.

As mentioned earlier, the number of points that characterize a measurement derived major loop is twice the number of recordings used to obtain it. This is also true for the derived FORCs. This creates a set of quasi-static loops (major loop and FORCs) with 2 to $2N$ points. From all the derived loops, the major loop is not used in the fitting process; it is a parameter of the model. Although an FORC is characterized only by two points, it does not present hysteretic behavior (two points can only represent a line), the points can still be used in the fitting process. However, since such an FORC lacks the hysteretic behavior, three or more measurements have to be carried out to have at least one FORC with hysteretic behavior together with a major loop. Furthermore, the number of points used to fit the coefficients per FORC is the same as the number of recordings. These points define the lower part of the ascending branch (not including the lower tip) and the FORC's upper tip. These are known as significant points. The reconstructed FORCs of the M-4 transformer used in this paper are presented in Fig. 5.

To obtain coefficients y_0 – y_6 , an optimization routine is used to minimize the following expression:

$$\sum_{c=1}^{N-1} \sum_{p=1}^c [\Delta H_{p,c}(B_{p,c}) - \Delta H_{\text{calc}}(B_{p,c})]^2 \quad (17)$$

where c is the FORC number that is being compared ($c = 1$ and $c = N - 1$ correspond to the FORC characterized by two points and the next smaller FORC after the major

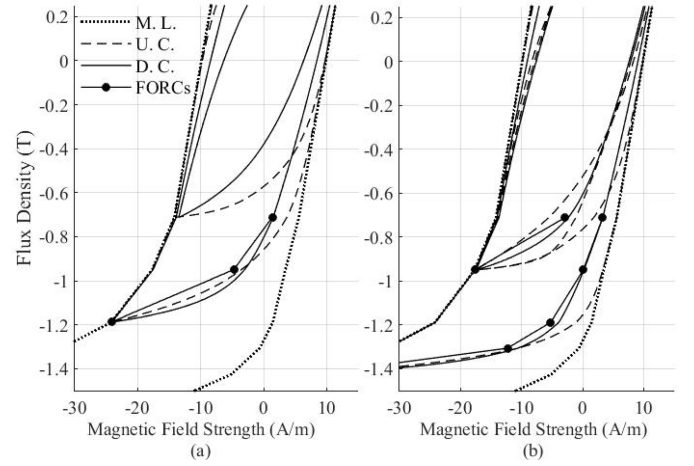


Fig. 6. FORCs comparison for different coefficients at different excitation levels. (a) 0.94 and 1.42 T. (b) 0.71 and 1.19 T. M. L. = Major Loop (dotted lines), U. C. = Undesirable Coefficients (dashed lines), and D. C. = Desirable Coefficients (continuous lines).

loop, respectively), p is the point number in the c th FORC, which is being used in the optimization problem, $\Delta H_{p,c}(B_{p,c})$ is the distance of the magnetic fields strength at a given flux density between the major loop and the c th FORC at point p , and $\Delta H_{\text{calc}}(B_{p,c})$ is the model predicted distance for a given set of parameters for point p of the c th FORC. Such optimization utilizes (2)–(7) and the calculated significant points that are part of each FORC in Fig. 5.

Remember that the constraints $a > 0$, $0 \leq b \leq 1$, and $y_6 > 0$ (Section II) have to be met for (4)–(6). Hence, these constraints are to be set into the optimization routine. For (4), it is preferable to have a dynamic constraint, by which the bounds for coefficients y_0 – y_3 change in each iteration. These dynamic constraints are meant to keep (4) positive. If this is not possible to implement, a bounded solution $y_0 > 0$ is usually applicable. However, one has to check that (4) is positive for all β ($1 \geq \beta \geq 0$). For (5), the constraint $0 \leq y_4 \leq 1$ satisfies the required conditions. However, to get better results, it is recommended to set $y_5 > 0$. Note that $y_6 > 0$ is the constraint for (6).

Some optimization routines, such as simulated annealing algorithm used in this paper, start from random initial guesses to get the solution. Therefore, it is possible to get different coefficients every time that (17) is minimized. Hence, it is important to check that the obtained minor loops have the desired shape (as it is done in Fig. 6). It may be needed to solve (17) several times and select a desired solution. For example, Fig. 6 shows different loops for the same excitations. These loops were obtained by minimizing the same equation (17) yielding different coefficients every time. Fig. 6 also shows some of the loops that were not considered good fittings. Some of the coefficients may yield good matching at higher excitation levels but not at low, such as having a very low returning step or very fast decay at low excitations. Others may show a good behavior in the low and high ends, but show errors in the midexcitations. In our experience, only a few runs of (17), fewer than 5, are needed to get good results. The iterative process can be automated by

looking at the individual distances in (17), i.e., $[\Delta H_{p,c}(B_{p,c}) - \Delta H_{calc}(B_{p,c})]^2 \leq \xi \forall p, c$.

IV. PARAMETER CALCULATION OF DYNAMIC COMPONENTS

The calculation of the other two components, classical eddy current components (10) and excess losses (11), of the three-component model (1) is very easy if the dimensions of the core, lamination thickness, and number of turns are known. However, in the absence of these parameters, an approximation based on a statistical analysis is suggested in this paper.

A. Classical Eddy Current Component

Equation (10) is derived from Maxwell equations for thin laminations. It assumes that the magnetic field is the same at the boundaries perpendicular to the sheet plain and that the magnetic field density and its rate of change are constant inside the whole sheet [1]. The following expression is the equivalent in the V - I domain:

$$I_{cl}(t) = \left(\frac{d^2 l}{12 \rho A N^2} \right) \frac{d\lambda}{dt} = \frac{V}{R_{cl}} \quad (18)$$

where A is the cross-sectional area of the lamination, l is the average length of the lamination, N is the number of turns, and I_{cl} is the instantaneous eddy current. Equation (18) allows recovering the value of the eddy current resistance as follows:

$$R_{cl} = \frac{12 \rho A N^2}{d^2 l}. \quad (19)$$

When the dimensions of the core are not known, a statistical approximation can be made. References [2] and [8] state that the classical eddy current losses represent about 20% of the total core losses for GO materials at 50 or 60 Hz. To validate this, a comparison of the total core losses versus the classical losses defined by (10) was done for six different transformers with similar design characteristics as the one presented in this paper. On average, the classical eddy current loss represents 18% of the total core losses with a standard deviation of 4%. The highest losses were 25.5% and the lowest losses were 14.2%. One can conclude that at nominal voltage (most of the transformers are designed to operate between 1.4 to 1.7 T), a reliable approximation for eddy current losses P_{cl} would be $18\% \pm 2\%$ of the total open-circuit losses. Therefore, the resistance that represents the eddy current losses R_{cl} can be calculated as

$$R_{cl} = \frac{V_{RMS}^2}{P_{cl}} \quad (20)$$

where V_{RMS} is the rms rated voltage.

B. Excess Loss Component

Excess losses are the result of the interactions between large magnetic domains, compared with the lamination thickness. A detailed explanation can be found in [1].

Determination of excess losses based on (11) is a phenomenological approach [2], [3], and [8]. In fact, for the model presented in this paper, the excess loss component is a fitting component. This model has two general parameters: an α power coefficient and a $g(B)$ polynomial function with m terms given in (21), as shown at the bottom of this page, where G_{nm} are the polynomial's coefficients, B_{xF} are the boundaries for a given function, and g_x is the x th polynomial of the $g(B)$ function. α has a value smaller than unity. Experience shows that the best value is $\alpha = 0.5$, so that it also complies with the dependency of the excess losses with the square root of the excitation frequency [1]. On the other hand, the polynomial function is an even function, and it can be a composition of different domains or a single domain.

The number of components and the order of the polynomial have to be chosen to obtain $g(B)$. Although one is totally free to choose the number of elements, the polynomial has to be at least of second order and its coefficients have to be positive. A higher number of components or a higher polynomial order provides more degrees of freedom to fit the model. Next, using the distance between the dynamic recorded loops and the quasi-static and classical derivations (with the same excitation), one can fit (11) for $n(m)+1$ points. Although there is no best loop to select for all cases, a loop between rated and major loops is recommended. The fitting should be carried for different loops and choose the one that yields the best results.

The first coefficient to be calculated by fitting the coercive force of the major loop (when $B = 0$ and dB/dt is maximum) is G_{10} . Then, the remaining variables form n systems of m linear equations: $g_1 - g_n$ (each composed by $m \times m$ elements), which are to be solved.

Although (11) and (21) are B - H relations, the λ - i representation has exactly the same structure. This means that no core dimensions are needed and the fitting can be directly done with measurements on

$$I_{exc}(t) = \pm h(\lambda) |V|^\alpha \quad (22)$$

where $h(\lambda)$ has the same structure as (21) but in λ , I , and V domains. For the representation of R_{exc} as a circuit element, a non-linear resistor can be used. This resistor is dependent on

$$g(B) = \begin{cases} g_1 = G_{10} + \sum_{k=1}^m G_{1k} B^{2k} & \forall 0 \leq B \leq B_{1F} \\ g_2 = g_1(B_{1F}) + \sum_{k=1}^m G_{2k} (|B| - B_{1F})^{2k} & \forall B_{1F} < |B| \leq B_{2F} \\ \vdots & \\ g_n = g_{n-1}(B_{n-1F}) + \sum_{k=1}^m G_{nk} (|B| - B_{nF})^{2k} & \forall B_{n-1F} < |B| \leq B_{nF} \end{cases} \quad (21)$$

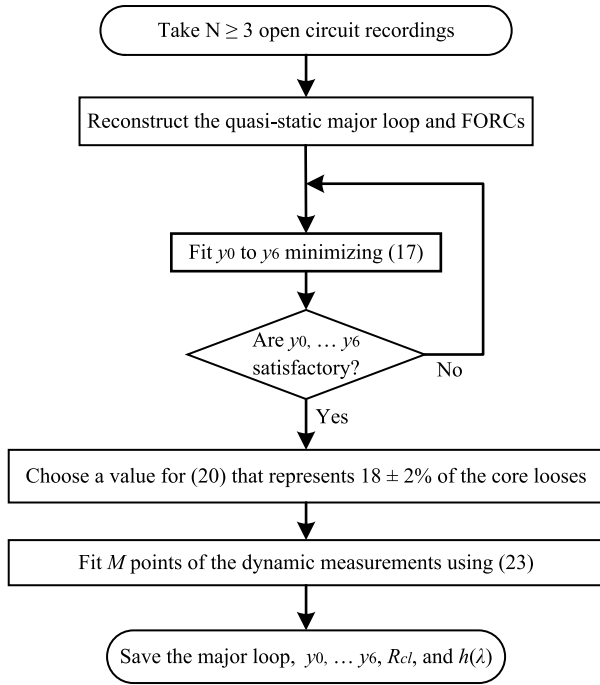


Fig. 7. Flowchart of the parameter determination method.

TABLE I
RECONSTRUCTION OF THE ASCENDING UPPER HALF
BRANCH OF THE QUASI-STATIC MAJOR LOOP

| Flux Peaks (T) | $H_a(B)$ (A/m) | $H(B, \dot{B})$ (A/m) | ΔH_+ (A/m) |
|----------------|----------------|-----------------------|--------------------|
| 0.71 | 14.18 | 30.69 | 16.51 |
| 0.95 | 17.68 | 35.67 | 17.99 |
| 1.19 | 24.17 | 44.33 | 20.15 |
| 1.31 | 32.07 | 52.12 | 20.05 |
| 1.42 | 44.40 | 66.18 | 21.78 |
| 1.54 | 78.91 | 98.44 | 19.53 |
| 1.60 | 116.50 | 135.65 | 19.15 |
| 1.66 | 183.20 | 206.52 | 23.32 |
| 1.69 | 249.21 | 267.16 | 17.95 |
| 1.73 | 374.75 | 374.75 | 0.00 |

the voltage and flux

$$R_{\text{exc}}(V, \lambda) = \frac{|V|^{1-\alpha}}{h(\lambda)}. \quad (23)$$

V. EXAMPLE

All the measured data, consisting of 12 dynamic loops, can be downloaded from [16]. Also posted are the MATLAB files of the fitted major loop, all FORCs, and the derived parameters used in this paper. Fig. 7 summarizes the procedure to compute the parameters as a flowchart. Tables I and II show the measured and calculated values for the variables needed to obtain the upper and lower ascending halves of the quasi-static major loop.

The next step is to obtain a set of FORCs. This is accomplished using the same procedure used for Tables I and II, but as mentioned in Section III-B, the upper measurements that were used have to be neglected to derive each FORC. With this

TABLE II
RECONSTRUCTION OF THE ASCENDING LOWER HALF
BRANCH OF THE QUASI-STATIC MAJOR LOOP

| Flux Peaks (T) | $H(B, -\dot{B})$ (A/m) | H_d (A/m) | $H_a(-B)$ (A/m) |
|----------------|------------------------|-------------|-----------------|
| 0.71 | -22.10 | -5.59 | 5.59 |
| 0.95 | -21.46 | -3.47 | 3.47 |
| 1.19 | -20.64 | -0.48 | 0.48 |
| 1.31 | -19.46 | 0.59 | -0.59 |
| 1.42 | -16.65 | 5.13 | -5.13 |
| 1.54 | -5.24 | 14.29 | -14.29 |
| 1.60 | 14.98 | 34.13 | -34.13 |
| 1.66 | 74.55 | 97.87 | -97.87 |
| 1.69 | 149.44 | 167.39 | -167.39 |
| 1.73 | 374.75 | 374.75 | -374.75* |

* This value has to be exactly the same as the peak $-H_a(B)$. Because measurements can have white noise of a very small magnitude, we recommend forcing this situation in the reconstruction.

TABLE III
FITTED COEFFICIENTS FOR DIFFERENT TRANSFORMERS,
MATERIALS, AND MEASUREMENT RESOLUTIONS

| | y_0 | y_1 | y_2 | y_3 | y_4 | y_5 | y_6 |
|----------|-------|--------|--------|-------|-------|-------|-------|
| M-4 Cat. | 7.13 | 2.26 | -25.7 | 41.83 | 1.0 | 0.38 | 2.3 |
| M-4 N=10 | 29.42 | -45.72 | -55.60 | 101.9 | 1.0 | 0.57 | 2.99 |

set of FORCs and using (17), the coefficients presented in the second row of Table III were computed. The initial conditions are taken from [3].

Classical eddy current losses are represented by a resistor, which referred into the B - H domain (10) has a value of 119.1 Ω/m . To fit the excess losses and for illustration, the following non-composite function of second order is used:

$$g(B) = G_{10} + G_{11}B^2 \quad (24)$$

where $G_{10} = 0.2$ and $G_{11} = 0.17$. These values were obtained fitting the rated loop at the coercive force for $B = 1$ T.

VI. MODEL VALIDATION

To validate this model, different situations were measured and reproduced: steady-state operation at different excitation levels at 60, 120, and 180 Hz and harmonic distorted excitation with minor loops.

As a measure of error, the relative and absolute differences of the total energy per cycle are presented in Fig. 8 for the 60, 120, and 180 Hz cases. One can appreciate large relative errors (15%) for low excitation at 120 Hz in Fig. 8(a). However, this is not a problem because the absolute error plotted in Fig. 8(b) is very small. Similarly, large absolute errors can be observed from Fig. 8(b) for 1.7 T, but the differences are not very large in relative terms.

A. Steady-State Operation at 60, 120, and 180 Hz

Fig. 9 shows a comparison between eight different measurements with the model using the same excitations, from 0.24 to 1.73 T (major loop). Two sets of calculations are shown, with and without compensation for eddy currents above saturation. One can see that the loops below the saturation knee (1.5 T) and over 30% of the saturation knee (0.47 T) are

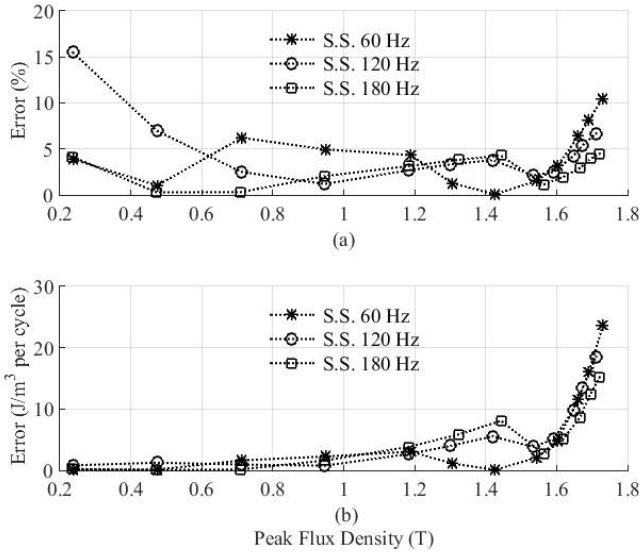


Fig. 8. Energy errors per cycle in (a) percentage and (b) energy density, between the simulated and measured loops at different excitations.

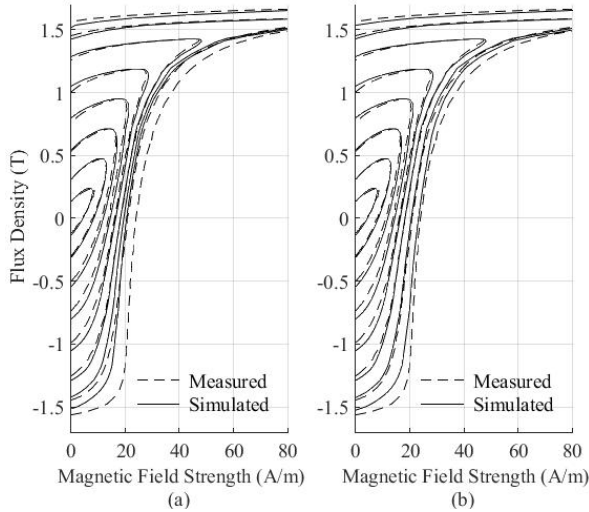


Fig. 9. Comparison of simulated versus measured dynamic hysteresis loops at different excitation levels at 60 Hz (a) without eddy current compensation and (b) with eddy current compensation.

in very good agreement with the measurements. The reason for the differences of the simulated loops for excitations close to saturation in Fig. 9(a) is related to the fact that (10) does not correctly represent the behavior of classical losses in a material operating under saturation conditions. In saturation conditions, the magnetization curve can be ideally seen as a steplike function and its classical field does not follow (10) anymore, but the eddy current losses are 1.5 times larger. More details can be found in [1, Sec. 12.2.3]. Reference [17] presents a solution to treat this problem.

To compensate for this, the classical eddy component for curves above 1.4 T is multiplied by the following factor:

$$1 + 0.5 \left[\frac{(B_{\text{peak}} - 1.4)}{(1.73 - 1.4)} \right]. \quad (25)$$

Although at 1.73 T the material is not yet in saturation, we can assume that it is, since in this condition, the permittivity is

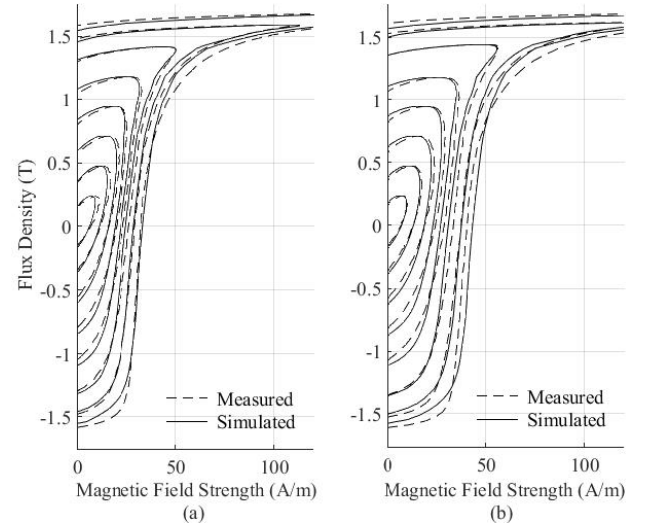


Fig. 10. Simulated versus measured comparison of dynamic loops at different excitations. (a) 120 Hz. (b) 180 Hz.

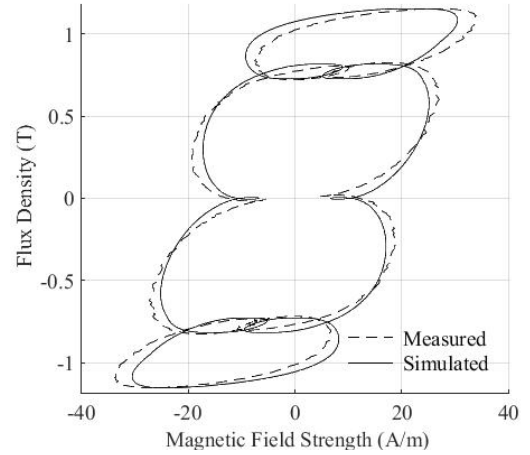


Fig. 11. Comparison between measured and simulated loops with an excitation with a high seventh-harmonic component.

low and the current is about 37 times larger than the coercive force of the quasi-static loop.

The cases of sinusoidal steady state excitation with 120 and 180 Hz are shown in Fig. 10. Excitation ranges from 0.24 to 1.73 T (major loop) peak. As in the case of 60 Hz, the loops are in very good agreement for the same range. This simulation already accounts for the eddy current compensation.

The model could be further improved using a higher order model for (14) or using a composite function, and include (25) in the fitting process. Using the following coefficients: $G_{10} = 0.19$, $G_{11} = 0.16$, and $G_{12} = 0.06$, the relative error is reduced to less than 6% for all excitations above 1.4 T for the three cases.

There is no published literature suggesting that excess losses present the same behavior. Nevertheless, the model improved its behavior when excess component was multiplied by $(1.5)^{0.5}$. The results are not presented because of the lack of scientific justification.

B. Harmonic Distorted Excitation

Fig. 11 shows a comparison of the model versus measurements with the following voltage excitation:

$$v(t) = 118 \sin(\omega t) + 130 \sin(7\omega t); \quad \omega = 2\pi f. \quad (26)$$

The energy has an error of about 2%. The model represents very accurately excitations that include very large harmonic components.

VII. CONCLUSION

A procedure to obtain all the needed parameters of the IHM dynamic model from terminal measurements has been presented. This includes a methodology to reconstruct the quasi-static loop solely from 60 Hz open-circuit recordings, which can be used for any model that requires a quasi-static loop. The classical eddy current component was statistically approximated for M-4 materials and the excess loss model was generalized.

The model has been validated against measurements at 60, 120, and 180 Hz for different excitation levels and with a signal composed by a fundamental and a large seventh harmonic. The results are in very good agreement between the model and measurements. An almost perfect match was obtained for excitations between 25% and 100% of the knee point. At higher excitation levels, the model presents loops with thinner hysteresis loop (lower losses). The differences have been traced to the representation of the eddy current losses for excitations close to saturation.

ACKNOWLEDGMENT

The authors would like to thank Prof. S. E. Zirka from Dnepropetrovsk National University, Ukraine, for his help understanding the model and for sharing important information. The first author would like to thank Consejo Nacional de Ciencia y Tecnología (CONACYT) and Comisión México-Estados Unidos (COMEXUS) for economic support of his M.Sc. studies at NYU making this work possible. This work was also supported by the National Science Foundation under Grant 1521233, awarded to Highest Transformers Inc. and NYU. Any opinions, findings, and conclusions or recommendations expressed in this material are those of the authors and do not necessarily reflect the views of the National Science Foundation.

REFERENCES

- [1] G. Bertotti, *Hysteresis in Magnetism*. San Diego, CA, USA: Academic, 1998.
- [2] S. E. Zirka, Y. I. Moroz, A. J. Moses, and C. M. Arturi, "Static and dynamic hysteresis models for studying transformer transients," *IEEE Trans. Power Del.*, vol. 26, no. 4, pp. 2352–2362, Oct. 2011.
- [3] S. E. Zirka, Y. I. Moroz, R. G. Harrison, and N. Chiesa, "Inverse hysteresis models for transient simulation," *IEEE Trans. Power Del.*, vol. 29, no. 2, pp. 552–559, Apr. 2014.
- [4] G. Gruosso and M. Repetto, "Identification method for a circuit model of scalar static hysteresis," *IEEE Trans. Magn.*, vol. 40, no. 6, pp. 3467–3473, Nov. 2004.
- [5] E. P. Dick and W. Watson, "Transformer models for transient studies based on field measurements," *IEEE Trans. Power App. Syst.*, vol. PAS-100, no. 1, pp. 409–419, Jan. 1981.

- [6] J. G. Frame, N. Mohan, and T.-H. Liu, "Hysteresis modeling in an electro-magnetic transients program," *IEEE Trans. Power App. Syst.*, vol. PAS-101, no. 9, pp. 3403–3412, Sep. 1982.
- [7] S. E. Zirka, Y. I. Moroz, N. Chiesa, R. G. Harrison, and H. K. Høidalen, "Implementation of inverse hysteresis model into EMTP—Part I: Static model," *IEEE Trans. Power Del.*, vol. 30, no. 5, pp. 2224–2232, Oct. 2015.
- [8] S. E. Zirka, Y. I. Moroz, N. Chiesa, R. G. Harrison, and H. K. Høidalen, "Implementation of inverse hysteresis model into EMTP—Part II: Dynamic model," *IEEE Trans. Power Del.*, vol. 30, no. 5, pp. 2233–2241, Oct. 2015.
- [9] A. Salvini, F. R. Fulginei, and G. Pucacco, "Generalization of the static Preisach model for dynamic hysteresis by a genetic approach," *IEEE Trans. Magn.*, vol. 39, no. 3, pp. 1353–1356, May 2003.
- [10] *Rule Book, Alternative Transient Program*, Comité Argentino de Usuarios de EMTP-ATP, Apr. 2002.
- [11] J. A. Garcia and M. Rivas, "A quasi-static magnetic hysteresis loop measurement system with drift correction," *IEEE Trans. Magn.*, vol. 42, no. 1, pp. 15–17, Jan. 2006.
- [12] J. R. Rhee *et al.*, "A bipolar pulse-type hysteresis loop tracer for rare earth based permanent magnets," *IEEE Trans. Magn.*, vol. 34, no. 4, pp. 2018–2020, Jul. 1998.
- [13] *Carlite Grain Oriented Electrical Steels M-3 M-4 M-5 M-6 Product Data Bulletin*, Apr. 2013, AK Steel, 9227 Centre Point Drive, West Chester, Ohio, USA.
- [14] D. E. Wiegand and W. W. Hansen, "A 60-cycle hysteresis loop tracer for small samples of low-permeability material," *AIEE Trans.*, vol. 66, no. 1, pp. 119–133, 1947.
- [15] W. Manly, Jr., "A 5.5-kOe 60-Hz magnetic hysteresis loop tracer with precise digital readout," *IEEE Trans. Magn.*, vol. 7, no. 3, pp. 442–446, Sep. 1971.
- [16] (Apr. 2016). *Measurements and Derived Parameters.Rar*. [Online]. Available: <https://www.mediafire.com/?3z8v96kfkjz9d>
- [17] S. Steentjes, S. E. Zirka, Y. E. Moroz, E. Y. Moroz, and K. Hameyer, "Dynamic magnetization model of nonoriented steel sheets," *IEEE Trans. Magn.*, vol. 50, no. 4, Apr. 2014, Art. no. 7300204.

Carlos H. Alonso was born in Irapuato, Mexico, in 1990. He received the bachelor's degree in electrical engineering from the Instituto Tecnológico de Morelia, Morelia, Mexico, in 2013, and the M.Sc. degree in electrical engineering from New York University, New York, NY, USA, in 2016.

His current research interests include transformer modeling and electro-magnetic transients.

Saeed Jazebi (S'10–M'14–SM'16) received the B.Sc. degree from the Shahid Bahonar University of Kerman, Kerman, Iran, in 2006, the M.Sc. degree from the Amirkabir University of Technology, Tehran, Iran, in 2008, and the Ph.D. degree from New York University, Brooklyn, NY, USA, in 2014, all in electrical engineering.

He has been a Post-Doctoral Fellow with New York University for two years. He is involved in research and development of fault current limiters and their applications in smart power systems with Applied Materials Inc., Gloucester, MA, USA. His current research interests include energy optimization, smart operation of power systems, electromagnetic design, modeling and simulation of electrical machines and power system components, power system protection, and power quality.

Francisco de León (S'86–M'92–SM'02–F'15) received the B.Sc. and M.Sc. degrees (Hons.) from the National Polytechnic Institute, Mexico City, Mexico, in 1983 and 1986, respectively, and the Ph.D. degree from the University of Toronto, Toronto, ON, Canada, in 1992, all in electrical engineering.

He has been with Canadian Electric Industry. He has held several academic positions in Mexico. He is currently an Associate Professor with the Department of Electrical and Computer Engineering, New York University, New York, NY, USA. His current research interests include the analysis of power phenomena under nonsinusoidal conditions, the transient and steady-state analyses of power systems, the thermal rating of cables and transformers, and the calculation of electromagnetic fields applied to machine design and modeling.

Prof. de León is an Editor of the IEEE TRANSACTIONS ON POWER DELIVERY and the IEEE POWER ENGINEERING LETTERS.